Environmental Science and Pollution Research (2021) 28:57166–57182
https://doi.org/10.1007/s11356-021-14626-7

RESEARCH ARTICLE

# Performance comparison of ejectors in ejector-based refrigeration cycles with R1234yf, R1234ze(E) and R134a

Shizhen Li[1] · Yingxin Liu[1] · Yanjun Liu[1,2] · Jingzhi Zhang[3]

Received: 13 November 2020 / Accepted: 25 May 2021 / Published online: 4 June 2021


## Abstract

To look for new refrigerants replacing R134a, environmentally friendly refrigerants R1234yf and R1234ze(E) were chosen as the alternatives in an ejector refrigeration system. The tested system contained a single-phase ejector, and numerical analysis regarding the performance of the ejector was done by CFD. The entrainment ratio, static pressure and Mach number were chosen as indicators revealing the ejector performance. Changes of the indicators of ejector utilizing a given refrigerant under varying operating temperature conditions were analysed. With the increasing condenser temperature, the shocking position moved upstream until it combined with the first series of oblique shocks. With the increasing generator temperature, the entrainment ratio increased firstly and decreased subsequently. With the increasing evaporator temperature, the primary-fluid jet expansion weakened. Comparisons of the indicators of ejector utilizing three working fluids (R134a, R1234yf and R1234ze(E)) under a given operating temperature condition were also made. The results showed that R1234yf had a greater entrainment ratio than R134a and R1234ze(E). But the shocking position of R1234yf was also closer to the upstream than the other two refrigerants, which caused the smaller critical mode region. Compared with the entrainment ratio close to 1.4 times, the critical temperature difference of only 3 °C could not weaken the advantages of R1234yf. Besides, heat transfer inside the ejector was considered and not much different trends with the three working fluids were found. Therefore, R1234yf could be the better candidate for R134a in the ejector refrigeration system.

**Keywords** Single-phase ejector · Numerical analysis · Entrainment ratio · Shocking position · Hypothetical throat · Expansion angle · Heat transfer

## Introduction

In 1858, Henry Giffard invented a condensing-type ejector to feed liquid water to steam engine boilers. Since then, supersonic ejectors have received considerable attention because they have no moving parts and no direct consumption of mechanical energy. Nowadays, it has been well applied for a wide range of applications, such as air conditioning, aerospace, natural gas exploitation and nuclear power.

In the refrigeration industry, the simplest form of refrigeration was the compressor refrigeration system which includes a compressor demanding a heavy load on electricity to lift the refrigerant pressure. To reduce the dependence on high-grade energy, Sokolov and Hershgal (1991) proposed an enhanced ejector refrigeration cycle, which could be activated by renewable sources or waste heat. Since then, a series of work cover the ejector refrigeration system had been carried out. More and more literatures proved the advantages of the application of ejectors, such as high reliability, durable life span and little maintenance cost (Expósito Carrillo et al. 2017; Megdouli et al. 2017; Kumar et al. 2020; Mondal and De 2020; Pérez et al. 2021), which was beneficial to its commercial application. There were many scholars researching how to improve the relatively low COP (coefficient of performance) of the ejector refrigeration system. For example, Sanaye et al. (2019), Elakhdar et al. (2018) and Cheng et al. (2021) had studied combining the ejector cycle with

Responsible Editor: Philippe Garrigues

✉ Jingzhi Zhang
zhangjz@sdu.edu.cn

[1] Institute of Marine Science and Technology, Shandong University, Qingdao 266237, China

[2] School of Mechanical Engineering, Shandong University, Jinan 250061, China

[3] School of Energy and Power Engineering, Shandong University, Jinan 266237, China

other systems such as the vapor compression cycle. Besides, some scholars, such as Sieres and Santos (2018) and Yilmaz and Erdinç 2019), had found that the type of working fluids could affect the great VCC (volumetric cooling capacity), COP and exergy efficiency of the system. With the restrictions from European Directive 2006/40/EC (Union and Parliament 2006), most researches involved the applications of CFCs (chlorofluorocarbons) and HFCs (hydrofluorocarbons) instead of R134a. Fang et al. (2017) pointed that R1234yf appeared to be a good candidate for drop-in replacement of R134a in an ejector heat-driven refrigeration cycle. And, a better entrainment ratio using R1234ze(E) could be obtained when maintaining the same pressure ratio for the ejector. In the study of Besagni et al. (2020a), the results showed that R134a, R1234yf and R1234ze(E) both had an intermediate value of COP. According to Galindo et al. (2020), R1234yf exhibited the best performance in terms of overall system efficiency closely followed by R600a and R1234ze(E). Besides, Mwesigye and Dworkin (2018) investigated the better performance of R1234ze(E) than R134a. Pabon et al. (2020) considered R1234yf as a promising substitute for R134a with GWP < 1. All the findings reveal that R1234yf and R1234ze(E) could be taken into account as the candidates.

As a key component of the system, the performance of the ejector plays a decisive role in that of the system. Experimental researches and numerical simulations of ejectors are gradually mature. As early as 1950, Keenan and Neumann (1950) introduced the constant-pressure mixing ejector based on the mass equation, momentum equation and energy equation. Under the constant-pressure mixing theory, Munday and Bagster (1977) pointed that the primary steam did not immediately mix with the secondary fluid until it causes an aerodynamic throat. According to Huang et al. (1999), the mixing took place inside the constant-area section. With the development of CFD (computational fluid dynamics), the mixing theory is validated and the inner flow behaviour becomes visible. Mazzelli et al. (2018), Han et al. (2019) and Mahmoudian et al. (2020) both exhaustively described the flow characteristics and mixing process in an ejector by CFD. Sriveerakul et al. (2007) discussed the phenomena on choke flow, mixing behaviour, jet core effect and the presence of oblique shock. Tang et al. (2020) systematically discussed the evolution laws of the mixing layer growth, the entrainment performance and the mass transfer of two streams. Actually, the accuracy of the ejector's visualization depends on the model settings, such as turbulence model, geometrical modelling and solvers. Bartosiewicz et al. (2005) compared five turbulence models to find the most suitable one in mixing phenomena prediction. Results showed that the k-ω SST turbulence model was the best one, which matched the discussion in Oliveira Marum et al. (2021). Additionally, Mazzelli et al. (2015) and Besagni et al. (2020b) found the good agreement of 2D and 3D models at on-design conditions, and there were no significant differences between density-based and pressure-based solvers. These findings laid the foundation for the development of better methods to design the ejector.

On the one hand, there are many literatures looking for friendly refrigerants that can replace R134a in the refrigeration systems, but they only compare the entrainment ratio and COP. On the other hand, the research on optimizing the ejector performance through the internal flow behaviour is also gradually maturing. However, there are not enough researches on the microscopic analysis of the difference in the internal flow behaviour of the ejector with different working fluids. Hence, a study to extend previous studies was performed. The main contributions of this paper are summarized as follows:

(i) Like most studies, the effects of temperature boundaries on the entrainment ratio, primary and secondary mass flow of the ejector utilizing R1234yf have been evaluated. Differently, the internal static pressure distribution, Mach number distribution and Mach number contour of the ejector obtained by CFD under different temperature conditions are listed to better explain the change of entrainment ratio. Besides, the internal flow behaviours of the ejector such as the shocking position, hypothetical throat and expansion angle are explained via Mach number contours.
(ii) Two low-GWP refrigerants (R1234yf and R1234ze(E)) were selected as the replaced fluids of R134a. The profiles of the entrainment ratio, primary and secondary mass flow rates, static pressure and Mach number of the ejectors utilizing different refrigerants under the same operating temperature are compared. Similarities and differences among the three refrigerants about the ejector performance are used to find the better candidate in the ejector refrigeration system.
(iii) Creatively, the temperature fluctuation caused by the mixing of two fluids with different temperatures is considered. The existence of temperature fluctuations proves the rationality of shock waves. Furthermore, the internal temperature distributions of the ejector utilizing the three working fluids under the same temperature boundary are analysed. This content is mainly used to prove whether temperature fluctuations can cause thermal strain and affect the choice of refrigerant.

## System description

### Ejector refrigeration system

As an ideal alternative to the compressor refrigeration system, the conventional ejector refrigeration system has higher energy efficiency and maintains the simplicity of the system. As shown in Fig. 1, the ejector refrigeration system introducing an ejector can be divided into two cycles, a forward cycle (1-2-3-4-1) and a

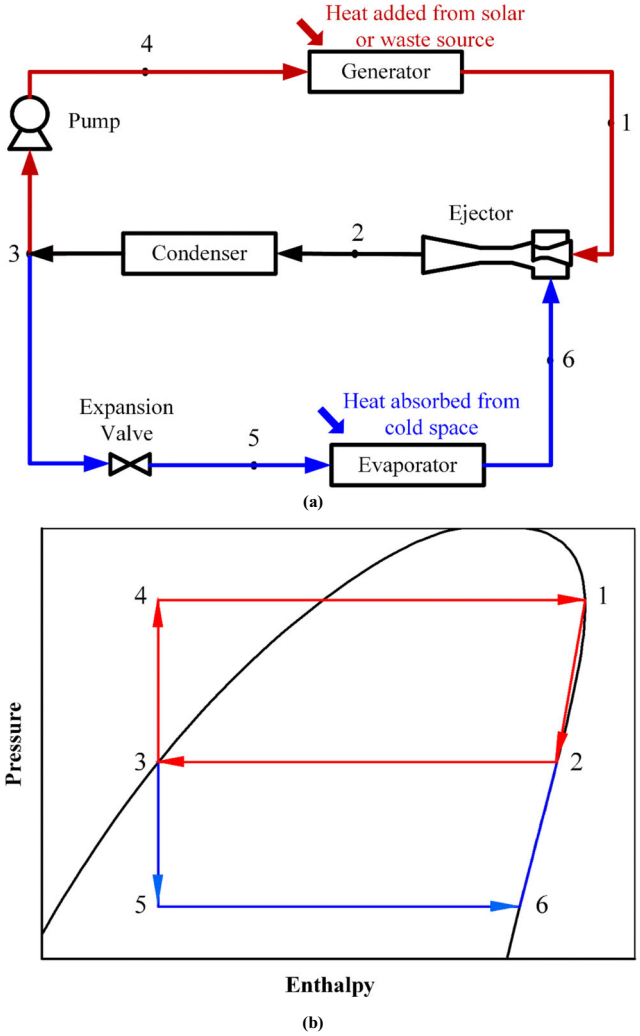


**Fig. 1** The **(a)** schematic diagram adapted from Rogdakis and Alexis (2000) and **(b)** pressure-enthalpy diagram omitting the changes in the ejector's internal enthalpy of the ejector refrigeration system

reverse refrigeration cycle (2-3-5-6-2). The reverse refrigeration cycle is still of much similarity with the compressor refrigeration system. The liquid refrigerant (state 3) obtained by the cooling of the condenser performs isenthalpic pressure reduction in the expansion valve. Then the depressurized refrigerant (state 5) enters the evaporator where the refrigerant absorbs external heat to lower the ambient temperature. Differently, the endothermic vaporization refrigerant (state 6) does not be compressed by the compressor, but enters the ejector where the pressure boost and speed boost could be realized. It should be noted that the completion of the ejector work requires the high-temperature and high-pressure gas (state 1) as a power source. This powered fluid, from one part of the cooling refrigerant (state 3), is got after the pressure boost pump and the heating generator. The existence of the ejector enables the refrigerant flowing through the evaporator to be pressurized without consuming external work. This is beneficial to reduce the power consumption of the compressor and increase the refrigeration efficiency.

## Ejector

As the main component of the system, the ejector connected with the generator, evaporator and condenser receives widespread attention. As depicted in Fig. 2, a classic ejector is composed of four sections, suction nozzle, mixing section, constant-area section and subsonic diffuser. The high-temperature and high-pressure gas from the generator is the primary fluid ($P_{pri}$, $t_g$, $\dot{m}_{pri}$) flowing into the primary nozzle. The endothermic vaporization refrigerant from the evaporator is the secondary fluid ($P_{sec}$, $t_e$, $\dot{m}_{sec}$) entering into the secondary inlet. After accelerating in the primary nozzle, the primary fluid expands and forms a low-pressure region at the exit of the nozzle. The pressure difference between the secondary inlet and the low-pressure region causes the secondary fluid to be entrained. As mentioned in He et al. (2009), the primary fluid does not immediately mix with the secondary fluid because of the large velocity difference. Instead, the primary flow flowing into the mixing chamber with an expansion angle creates an entrained duct to accelerate the secondary fluid (Chunnanond and Aphornratana 2004). As shown in Fig. 2, the two fluids do not start mixing until they reach the cross-section a-a (named the hypothetical throat). As the mixing process proceeds, the speed of the secondary fluid increases to a sonic value and the effective area of it reaches the minimum. Subsequently, the two fluids reach the constant-area section at a uniform static pressure. At cross-section b-b (named the shocking position), compression shock waves are induced and cause a sudden increase in pressure. Before entering the subsonic diffuser, the two fluids completely mix and have the same velocity. Ultimately, the well-mixed fluid is compressed in the subsonic diffuser and discharged into the condenser ($P_{out}$, $t_c$, and $\dot{m}_{out}$).

Many studies (Petrovic et al. 2018; Varga et al. 2013; Biferi et al. 2016) illustrated that three working modes, the critical mode, subcritical mode and back-flow mode, could be observed by varying the back pressures. However, the ejector in the ejector refrigeration cycle is directly connected with the generator, evaporator and condenser, which makes the temperature of the refrigerant is easier to control than its pressure. Besides, refrigerants flowing through the ejector are both saturated gases to ensure a single-phase operation of the ejector. According to the one-to-one correspondence between temperature and pressure expressed by the ideal gas equation, the condenser temperature instead of the back pressure is selected as the independent variable. As shown in Fig. 3, entrainment ratio ($\omega$) characterizing the working states of the ejector is the dependent variable, which is defined as

$$\omega = \frac{\dot{m}_{sec}}{\dot{m}_{pri}} \tag{1}$$

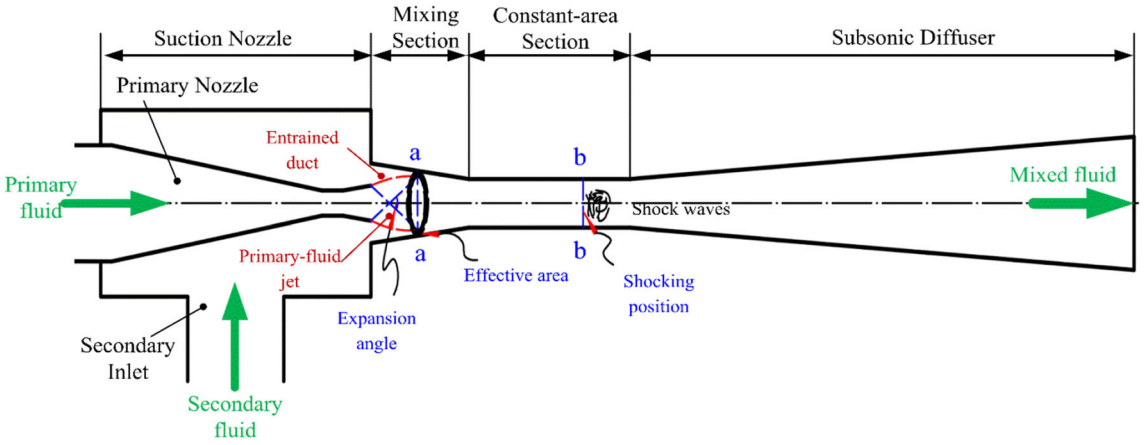


**Fig. 2** Structure diagram of the typical ejector

where $\dot{m}_{pri}$ is the mass flow rate of the primary fluid, $\dot{m}_{sec}$ is the mass flow rate of the secondary fluid. When the condenser temperature does not exceed the critical value, the entrainment ratio remains constant. But when it increases beyond the critical point, the entrainment ratio will decrease to a negative value.

## Numerical model and validation

### Ejector geometry

In order to explore the difference of the ejectors utilizing R134a, R1234yf and R1234ze (E) respectively, the ejector proposed by Yan et al. (2012) is chosen as reference. Similar to the study of Yan et al. (2012), this paper pays attention to the ejectors in refrigeration systems and chooses R134a as the one working fluid. Differently, the main dimensions of the ejector in this article have changed, which are listed in Table 1.

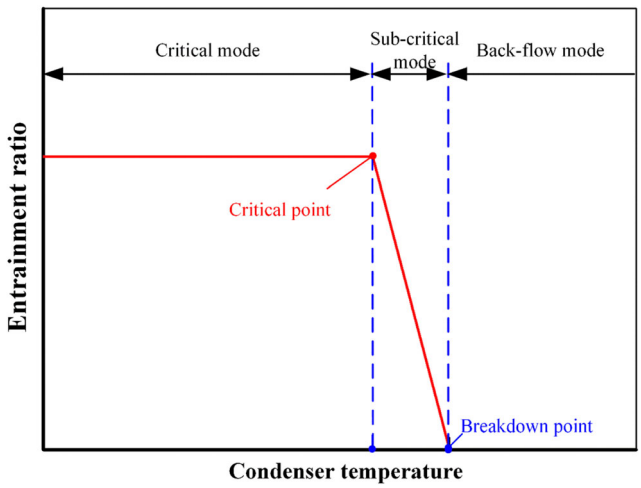


**Fig. 3** Variations of entrainment ratio with condenser temperature

## Governing equations

A brief review of models in the literature will be carried out to made reasonable assumptions reducing the complexity of the calculation. In the study of Keenan and Neumann (1950), an ejector design method assuming the fluid as ideal gas was presented. Equations of mass, momentum and energy balance were founded to define the flow through the ejector. In this case, numerical values in agreement with that of the experiment were obtained, but the double choking of ejectors could not be represented. To make up for the drawback, Munday and Bagster (1977) supposed that the primary fluid expanded out of the primary nozzle remaining unmixed with the secondary fluid. Until reaching the hypothetical throat where the secondary fluid was accelerated to a sonic velocity, the two fluids started mixing. Huang et al. (1999) discussed a single-phase ejector by assuming the fluid as an ideal gas. They believed that the mixing occurred at a uniform pressure. Sriveerakul et al. (2007) discovered the shocking position existing in the ejector throat or in the beginning of the diffuser section. Dominated by the second series of oblique shock waves, the static pressure would recover to the discharged

**Table 1** Main dimensions of the simulated ejector

| Geometry parameters | Value [mm] |
|---|---|
| Primary nozzle throat diameter | 2.9 |
| Primary nozzle exit diameter | 4.5 |
| Primary nozzle exit position | 0 |
| Mixing section entry diameter | 8 |
| Mixing section length | 14 |
| Constant-area section diameter | 5.5 |
| Constant-area section length | 23 |
| Subsonic diffuser exit diameter | 15 |
| Subsonic diffuser length | 72 |

value gradually. In terms of the theory of constant pressure mixing, the following assumptions are made:

- The flow inside the ejector is a single-phase flow, and the inner wall of the ejector is adiabatic.
- The flow inside the ejector is in a steady state.
- The working fluid is an ideal gas.
- The expanding primary-fluid jet creates a hypothetical throat, where the primary fluid and secondary fluid begin mixing.
- The shocking position occurs at the downstream of the constant-area section or at the beginning of the subsonic diffuser section.

Based on the above assumptions, the perfect gas model is used to obtain the fluid density, and the thermal and hydrodynamic fluid properties are assumed to be constant. The governing equations, which include the mass, momentum and energy conservation for the ejector, can be presented as follows.

Conservation of mass:

$$\frac{\partial \rho}{\partial t} + \frac{\partial}{\partial x_i}(\rho u_i) = 0 \tag{2}$$

Conservation of momentum:

$$\frac{\partial}{\partial x_i}(\rho u_i) + \frac{\partial}{\partial x_j}\left(\rho u_i u_j\right) = \frac{\partial \tau_{ij}}{\partial x_j} - \frac{\partial \rho}{\partial x_i} \tag{3}$$

Conservation of energy:

$$\frac{\partial}{\partial t}(\rho E) + \frac{\partial}{\partial x_i}\left[u_i(\rho E + P)\right] = \vec{\nabla}\cdot\left(\kappa_{eff}\frac{\partial T}{\partial x_i}\right) + \vec{\nabla}\cdot\left[u_j(\tau_{ij})\right] \tag{4}$$

with

$$\tau_{ij} = \mu_{eff}\left(\frac{\partial u_i}{\partial x_j} + \frac{\partial u_j}{\partial x_i}\right) - \frac{2}{3}\mu_{eff}\frac{\partial u_k}{\partial x_k}\delta_{ij} \tag{5}$$

where $\rho$ is density, $u$ is the velocity vector, $E$ is total energy, $P$ is pressure, $T$ is static temperature, $\kappa_{eff}$ is effective thermal conductivity, $\mu_{eff}$ is effective dynamic viscosity and $\delta_{ij}$ is the Kronecker delta function.

## Boundary conditions and mesh generation

To compute the performance of the single-phase supersonic ejector, the CFD package ANSYS Fluent 19.0 is adopted. The 3D calculation model is simplified to a 2-D axisymmetric symmetric model to save computational cost, which has been proven by Yan et al. (2012), Gu et al. (2017) and Wang et al. (2018). As shown in Fig. 4, the boundaries of the primary inlet and secondary inlet are set as pressure inlets, and the boundary of the outlet is the pressure outlet. The symmetry axis is set to axis, and the remaining boundaries are considered no-slip walls. Moreover, the pressure inlets and outlet are defined at saturated states, and the walls are adiabatic and smooth. In Gambit 2.4.6, the simulation model is meshed with the structural grid. Since there is a huge variation in velocity and pressure in the primary nozzle, mixing section and constant-area section, the meshes must be refined in this region. Meanwhile, boundary layers near the walls must be sufficiently intensive to capture the complicated working process.

In terms of the ejector's working system, the primary pressure inlet is generator pressure, the secondary pressure inlet is evaporator pressure, and the pressure outlet is condenser pressure. The specific pressure values are obtained by the ideal gas equation according to the corresponding temperatures. According to literatures about refrigeration systems, both the condenser temperature (30~55 °C) and evaporator temperature (− 20~15 °C) have universally feasible ranges. Differently, the generator temperature has no fixed range depending on the motivated heat and the refrigerant's critical temperature. On the basis of the tested fluids, operating conditions are set according to Table 2.

In many studies, grid density is one of the most effective parameters that affect the computational accuracy. Dynamic mesh adaption method is implemented to encrypt the grid, and grid spacing at the first layer of the walls follows the rules $30 \le y^+ \le 100$. Three types of meshes are evaluated: grid 1 with 58,683 cells, grid 2 with 133,658 cells and grid 3 with 366,552 cells. As shown in Fig. 5, curves of Mach number distribution along the axis of ejectors are very similar. As depicted in Table 3, the $\dot{m}_{pri}$, $\dot{m}_{sec}$ and $\omega$ of grid 1 are quite different from that of the other two, and the data of grid 2 and grid 3 are very close. The percentage difference of $\omega$ between grid 1 and grid 2 is up to 10.5%, while that between grid 2 and grid 3 is only 2.4%.

Besides, the *GCI* (grid convergence index), which is a standardized way to report grid convergence quality, is also considered. $\dot{m}_{sec}$ is chosen as the parameter indicator, and the refinement ratio is 1.5. All the calculated parameters are obtained by taking the example in John (2021) as a basis.

The order of convergence ($p$) is calculated as

$$p = \ln\left(\frac{f_3 - f_2}{f_2 - f_1}\right)/\ln(r) \tag{6}$$

where $r$ is the refinement ratio, $f_1$ is the $\dot{m}_{pri}$ of grid 3, $f_2$ is the $\dot{m}_{pri}$ of grid 2, $f_3$ is the $\dot{m}_{pri}$ of grid 1. Using the known data, $p$ is equal to 7.40.

The *GCI* is defined as

$$GCI = \frac{F\cdot|e|}{r^p - 1} \tag{7}$$

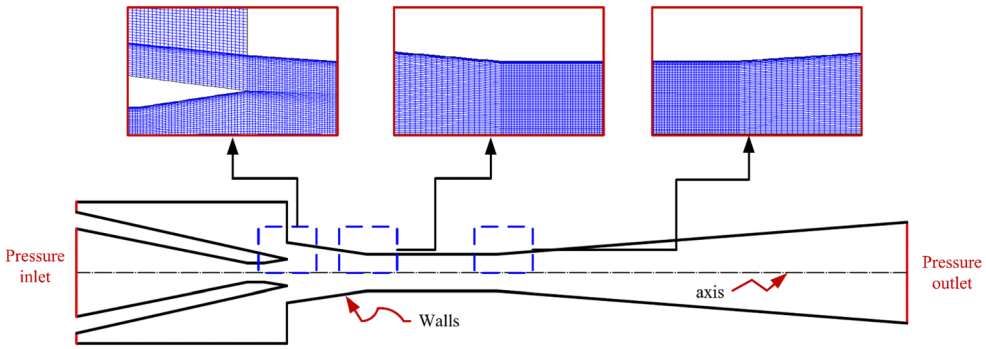


**Fig. 4** Computational domain and details of the grids

where $e$ is the difference of $\dot{m}_{pri}$ between two grides and $F$ is an optional safety factor ($F = 1.25$ for comparisons of three grids). Based on this equation, $GCI_{2,3}$ is equal to 0.66% and $GCI_{1,2}$ is equal to 0.03%.

With three grids, the grid convergence can be checked as

$$\frac{GCI_{2,3}}{r^p \cdot GCI_{1,2}} \approx 1 \tag{8}$$

The calculated value of the left-hand side of Eq. (8) is 1.0948, which indicates that the solutions are in the asymptotic range and they of grid independence. Considering the calculation accuracy and the time required, the grid with 133658 quadrilateral elements is sufficient to obtain the ejector performance.

## Case setup

After discretization, Fluent 19.0 is used to compute the steady-state, 2-D axisymmetric turbulent flow inside the ejector. R134a, R1234yf and R1234ze(E) are selected as the working fluids, whose densities are obtained by the ideal gas law and other thermal properties are collected from the REFPROP 9.1 (Lemmon et al. 2013) database. The second-order upwind scheme is selected to improve the numerical accuracy, and the well-known SIMPLE algorithm is used to obtain the pressure field. According to previous studies (Croquer et al. 2016; Mazzelli et al. 2015), the SST (shear stress trfansport) k~ω model is adopted due to its specific calibration for transonic applications. Besides, the result is not considered convergent until the residual of the energy equation is less than $10^{-8}$ and the net mass flux is less than $10^{-7}$. The related settings are shown in Table 4.

**Table 2** Operating conditions

| Parameters | Values | | |
|---|---|---|---|
| | R134a | R1234yf | R1234ze(E) |
| $t_g$ [°C] | 66~94 | 66~94 | 66~94 |
| $t_e$ [°C] | 3~15 | 3~15 | 3~15 |
| $t_c$ [°C] | 30~40 | 30~40 | 30~40 |

## Model validation

As the commonly used refrigerant of the refrigeration systems, there are many reliable experimental or numerical researches on R134a. In contrast, the experimental model data about the environmentally friendly refrigerants R1234yf and R1234ze(E) is not enough due to their late appearance. Most research on HFOs are still focused on their physical properties and simulations. In view of the similarities of R134a, R1234yf and R1234ze(E), a model validation only employing R134a is carried out before studying R1234yf and R1234ze(E). Facts (Fang et al. 2017; Mwesigye and Dworkin 2018) had been proven that this work was enough to provide detailed model data for HFO simulation calculations. The before-mentioned numerical methods are validated based on the experimental values from García del Valle et al. (2014). Three mixing chambers "A", "B" and "C", whose schematic diagrams are drawn in Fig. 6a, are compared. As displayed in Fig. 6b and

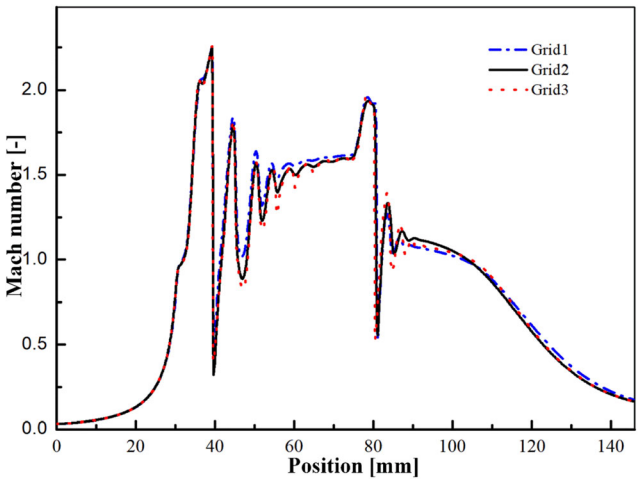


**Fig. 5** Mach number distribution along the axis of the ejector under different grid numbers

**Table 3** Comparisons of $\dot{m}_{pri}$, $\dot{m}_{sec}$ and $\omega$ for the ejector with three grids

| | $\dot{m}_{pri}$ [$\times 10^{-2}$ kg/s] | $\dot{m}_{sec}$ [$\times 10^{-2}$ kg/s] | $\omega$ [-] |
|---|---|---|---|
| Grid 1 | 5.18 | 1.98 | 0.38 |
| Grid 2 | 5.15 | 2.18 | 0.42 |
| Grid 3 | 5.15 | 2.19 | 0.43 |

Table 5, $\omega$ obtained from the CFD model is slightly different from that of the experimental investigation. The relative errors of most numerical simulation results and test results are within ± 10%. Therefore, this numerical method can adequately predict the ejector performance in the following simulation.

## Results and discussion

In this investigation, the geometric structure of the ejector in Fig. 2 and Table 1 is fixed, and the refrigerants and operating conditions are variables. Significant parameters such as entrainment ratio ($\omega$), Mach number, static pressure and temperature are selected to analyse the ejector performance.

### Effects of condenser temperature on the ejector performance

The presence of three working modes indicates that the critical condenser temperature is a key norm that determines the operating regimes of the ejector. Validations were conducted with three refrigerants. As shown in Fig. 7, each refrigerant displays a typical behaviour, which is consistent with Fig. 3. For the critical mode, $\omega$ of each refrigerant is independent of the condenser temperature and remains at the maximum value. After the critical point, each refrigerant will reach the subcritical mode with a decreasing $\omega$. Differently, whether $t_g$ is 86 °C or 94 °C, the greatest $\omega$ measured for R1234yf is always the maximum, and that of R1234ze(E) is the minimum. The difference between R1234yf and R1234ze(E) is approximately 25.5% ($t_g$ = 86 °C) and 34.8% ($t_g$ = 94 °C), respectively. In addition, with increasing $t_g$, each refrigerant will obtain a larger "critical mode" region, but this region of R1234yf is still smaller than those of R134a and R1234ze(E). However, the maximum difference is only 3 °C. Hence, R1234yf may be a better potential substitute for R134a because of its higher entrainment ratio.

**Table 4** Basic settings in Fluent 19.0

| Parameters | Values |
|---|---|
| Primary nozzle inlet | Pressure inlet |
| Secondary inlet | Pressure inlet |
| Ejector outlet | Outlet |
| Viscous model | SST k-ω model |
| Materials | R134a, R1234yf, R1234ze(E) |
| Pressure-velocity Coupling | SIMPLE |
| Spatial Discretization | Second-order upwind |

### Effects of generator temperature and evaporator temperature on the ejector performance

According to Eq. (1), $\omega$ is defined by $\dot{m}_{pri}$ and $\dot{m}_{sec}$, which are directly influenced by generator temperature and evaporator temperature. Thus, the effects of $t_g$ and $t_e$ are considered in the following discussion.

As presented in Fig. 8, the effects of the generator temperature on ejector performance are similar for these three refrigerants. With increasing $t_g$ (from 74 °C to 94 °C in steps of 2 °C), $\dot{m}_{pri}$ shows a linear growth trend, while $\dot{m}_{sec}$ first increases and subsequently decreases. The point where $\dot{m}_{sec}$ reaches a peak is called the optimum point, and its corresponding generator temperature is the optimal generator temperature. Before the optimum point, the ejector works at the subcritical mode, and more secondary fluid can be entrained by the increase of the primary fluid. Because $\dot{m}_{sec}$ increases faster than $\dot{m}_{pri}$, there is an increase in $\omega$. However, when $t_g$ exceeds the optimum value, there will be a drop in $\omega$ with increasing $\dot{m}_{pri}$ and decreasing $\dot{m}_{sec}$. Combined with Fig. 7, the area after the optimum point in Fig. 8c indicates that the ejector works in the critical mode. In the study of Atmaca et al. (2017), this region is called the operation range of $t_g$.

Similarly, for the effects of evaporator temperature on the ejector performance, all refrigerants show similar characteristics. As presented in Table 6, $\dot{m}_{pri}$ remains constant at different evaporator temperatures. When $t_e$ increases, more secondary fluid is entrained, which makes $\omega$ increase. The same result is obtained from Fig. 9a. When $t_e$ changes from 5 to 15 °C, a larger operation range of $t_g$ is observed for each refrigerant. However, Fig. 9b shows that when $t_c$ changes from 35 to 40 °C, both operation range of $t_g$ and maximum $\omega$ will decrease for the tested refrigerants.

There are still some differences among the three refrigerants. As shown in Fig. 8a and Table 5, R1234ze(E) always has the lowest $\dot{m}_{pri}$, while R134a and R1234yf have similar values. In the critical mode, R1234ze(E) has the minimum $\omega$, and R1234yf has the maximum $\omega$. Additionally, R1234yf has the highest optimal generator temperature, while R1234ze(E) has the smallest value. In other words, R1234yf has the smallest operation range of $t_g$ among the three refrigerants. However, at the optimum points, R1234yf obtains a $\omega$ value that is approximately 4.4% and 7.6% higher than those of R134a and R1234ze(E), respectively. Moreover, when the three refrigerants are under identical temperature conditions,

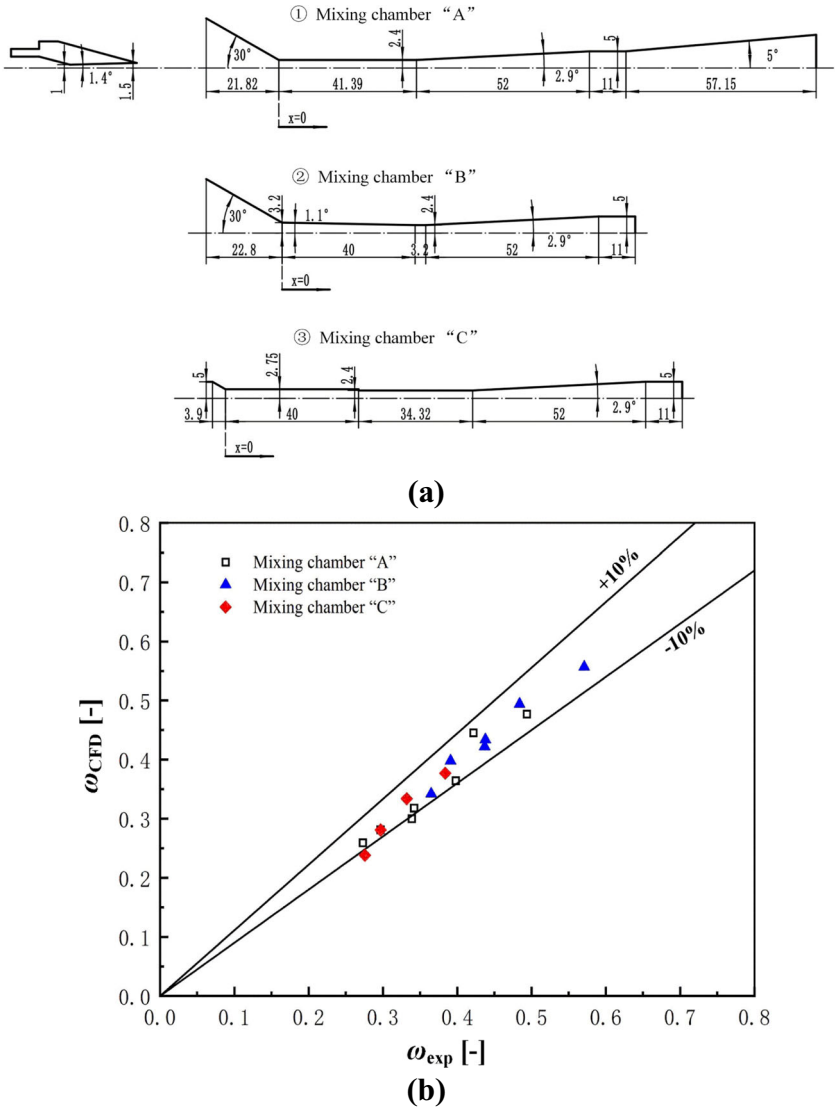


**Fig. 6** The schematic diagrams of **(a)** the geometries for the three mixing chambers "A", "B" and "C" which are adapted from García del Valle et al. (2014) and **(b)** entrainment ratios of the CFD model versus that of experiment

R1234yf has an $\omega$ approximately 14.8% higher than R134a. In conclusion, although R1234yf always has a smaller operation range of $t_g$, this disadvantage is not sufficient to offset the advantage that R1234yf has the highest $\omega$.

## Distributions of the static pressure and Mach number

From the previous analysis, variations of the operating conditions affect entrainment ratio, and this effect is not identical on

**Table 5** Entrainment ratios of CFD model and that of experiment (García del Valle et al. 2014)

| Generator | Evaporator | Mixing chamber "A" | | Mixing chamber "B" | | Mixing chamber "C" | |
|---|---|---|---|---|---|---|---|
| $t_g$ [°C] | $t_e$ [°C] | $\omega_{exp}$ [-] | $\omega_{CFD}$ [-] | $\omega_{exp}$ [-] | $\omega_{CFD}$ [-] | $\omega_{exp}$ [-] | $\omega_{CFD}$ [-] |
| 79.37 | 10 | 0.494 | 0.477 | 0.571 | 0.557 | – | – |
| 84.39 | 10 | 0.398 | 0.364 | 0.484 | 0.494 | 0.384 | 0.377 |
| 89.15 | 10 | 0.339 | 0.300 | 0.437 | 0.422 | 0.332 | 0.334 |
| 79.37 | 7 | 0.422 | 0.445 | – | – | – | – |
| 84.39 | 7 | 0.342 | 0.318 | 0.438 | 0.434 | – | – |
| 89.15 | 7 | 0.297 | 0.281 | 0.391 | 0.398 | 0.297 | 0.281 |
| 89.15 | 5 | 0.273 | 0.259 | 0.365 | 0.342 | 0.276 | 0.238 |

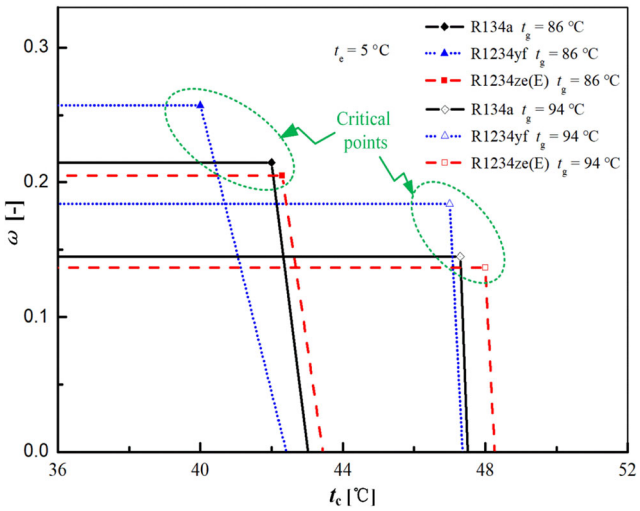


**Fig. 7** Variations of entrainment ratio with condenser temperature

the three refrigerants. This section utilizes static pressure and Mach number distributions to visualize the flow behaviour in ejectors to further explain these results.

Figure 10 presents the distributions of static pressure and Mach number of an ejector who utilizes R1234yf and works in the critical mode ($t_g$ = 86 °C, $t_c$ = 35 °C and $t_e$ = 5 °C). The primary fluid can accelerate to a supersonic state in the primary nozzle throat, and its pressure at the suction nozzle exit is lower than that of the secondary inlet. Hence, the secondary fluid is entrained and mixes with the primary fluid at the hypothetical throat. Later, the static pressure along the ejector wall basically remains constant until the fluids arrive at the shocking position. As shown in Fig. 10, fluctuations occur after two sudden changes in static pressure and Mach number. Sriveerakul et al. (2007) called them the first series oblique shocks and second series oblique shocks according to the order of appearance. The first series of oblique shocks start from the hypothetical throat where both Mach number and static pressure along the axis of the ejector reach the inflexion point for the first time. The second series oblique shocks begin at the shocking position after which both Mach number and static pressure along the axis of the ejector will have big changes. Then, the mixed fluid enters the subsonic diffuser and is further compressed. Ultimately, a well-mixed fluid with a higher pressure than the secondary inlet is discharged.

As depicted in Fig. 11, flow behaviours in ejectors operating in three working modes are simulated. Regardless of the change in $t_c$, the primary nozzle inner flow behaviour and hypothetical throat position do not change, which proves that an increase in $t_c$ has no effect on the primary fluid. When $t_c$ increases from 35 to 40 °C, the shocking position will move upstream. However, the rising shocking position is not sufficient to damage the choked secondary fluid. The ejector still works at the critical mode with constant ω. At $t_c$ = 42 °C and $t_c$ = 44 °C, only the primary fluids are choked, and there are no

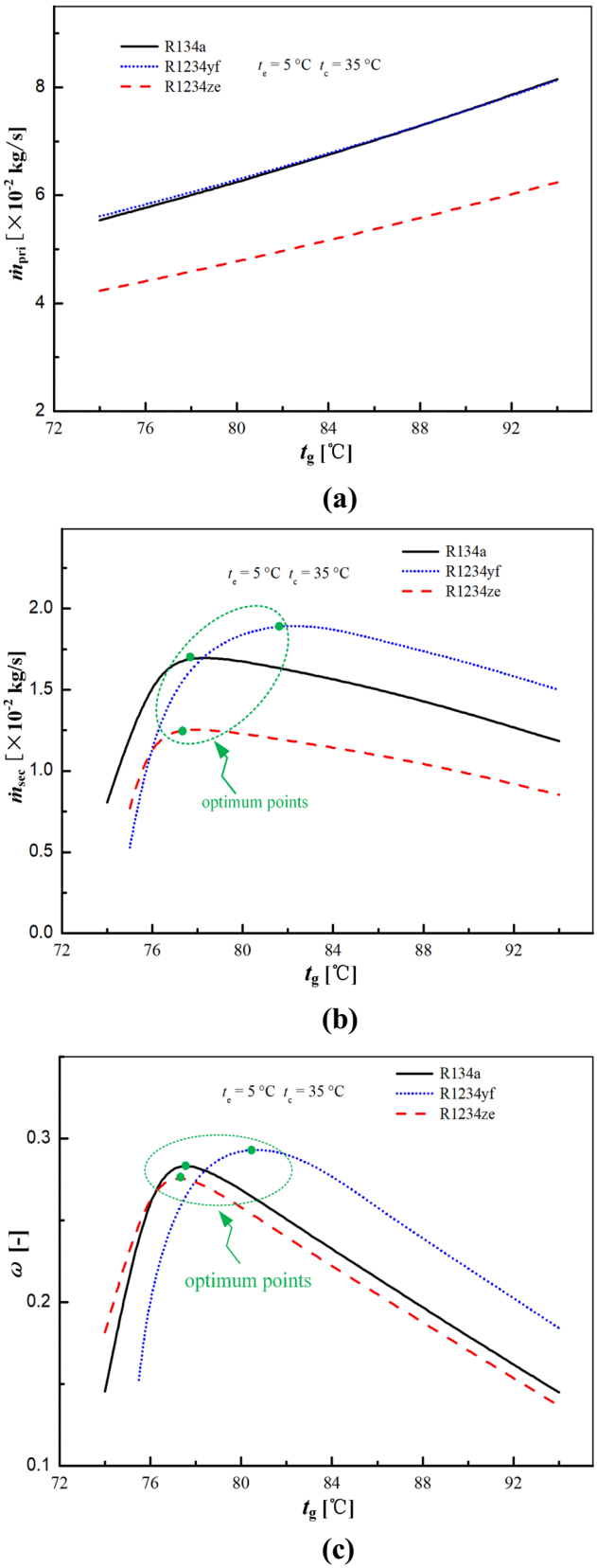


**Fig. 8** Effects of generator temperature on ejectors performance that includes **(a)** $\dot{m}_{pri}$, **(b)** $\dot{m}_{sec}$ and **(c)** ω with three refrigerants under $t_e$ = 5 °C, $t_c$ = 35 °C (All lines have received B-spline curve processing)

**Table 6** Comparisons of $\dot{m}_{pri}$, $\dot{m}_{sec}$ and $\omega$ for the three refrigerants

| Refrigerant | $t_e$ [°C] | $\dot{m}_{pri}$ [$\times 10^{-2}$ kg/s] | $\dot{m}_{sec}$ [$\times 10^{-2}$ kg/s] | $\omega$ [-] |
|---|---|---|---|---|
| R134a | 7 | 5.54 | 1.30 | 0.23 |
| | 10 | 5.54 | 1.84 | 0.33 |
| | 12 | 5.54 | 2.02 | 0.37 |
| | 15 | 5.54 | 2.34 | 0.42 |
| R1234yf | 7 | 5.61 | 0.22 | 0.04 |
| | 10 | 5.61 | 1.06 | 0.19 |
| | 12 | 5.61 | 1.72 | 0.31 |
| | 15 | 5.61 | 2.35 | 0.42 |
| R1234ze(E) | 7 | 4.23 | 1.05 | 0.25 |
| | 10 | 4.23 | 1.37 | 0.32 |
| | 12 | 4.23 | 1.48 | 0.35 |
| | 15 | 4.23 | 1.72 | 0.41 |

shocking positions. Meanwhile, the second series oblique shocks move upstream and combine with the first series oblique shocks. Differently, when the ejector works in the subcritical mode, its $\dot{m}_{sec}$ will decrease from the maximum to zero with no reverse flow. However, as shown in Fig. 11b, there will be a reversed-flow primary fluid via the secondary inlet when the ejector works in the back-flow mode. Consequently, as exhibited in Fig. 3 and Fig. 7, an increase in $t_c$ will make $\omega$ constant firstly and decrease subsequently. Thus, the condenser temperature affects the ejector performance by changing the choked secondary fluid.

Generator temperature and evaporator temperature have almost opposite effects on entrainment ratio. As shown in Fig. 12a, ejectors using R1234yf as the working fluid are working in the critical mode. Whether $t_g$ or $t_e$ increases, the shocking position inside the ejector will move downstream. However, an increase in $t_g$ causes a higher $\dot{m}_{pri}$ and makes the primary fluid leave the suction nozzle with a higher pressure, which increases the momentum of the primary fluid. As displayed in Fig. 12b, Primary-fluid jets (Mach number ≥ 1) of the three working fluids are compared. The closed curves (Mach number ≥ 2.2) represent the first series oblique shocks. The effective area (an annulus area which the secondary fluid passes) corresponds to $\dot{m}_{sec}$, which is similar to the definition mentioned in Metin et al. (2019). It can be found that the primary-fluid jet can fully expand due to the increasing $t_g$ and make the hypothetical throat move downwards. Therefore, a smaller expansion angle is obtained, and less secondary fluid can flow the annulus area. Although increasing $t_e$ cannot change its momentum due to the unchanged $\dot{m}_{pri}$ and unchanged pressure at the suction nozzle exit, it can increase the annulus area to limit the expansion of the primary-fluid jet. Thus, the hypothetical throat occurs earlier, and there is a smaller area of the primary-fluid jet.

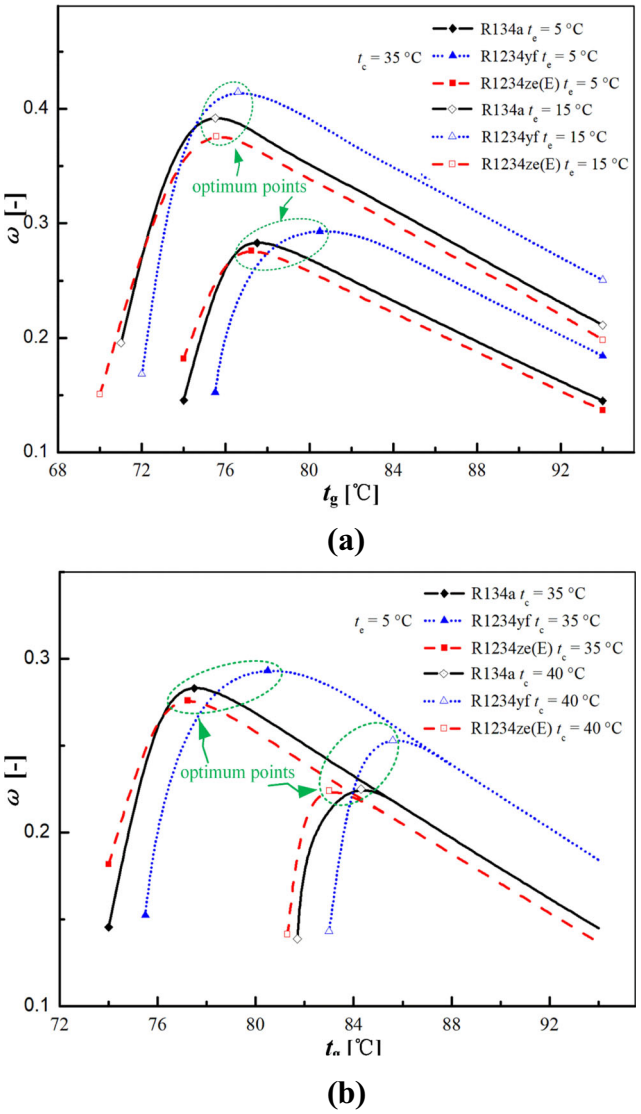


**Fig. 9** Effects of generator temperature on $\omega$ under **(a)** $t_e$ = 5 or 15 °C, $t_c$ = 35 °C and **(b)** $t_e$ = 5 °C, $t_c$ = 35 or 40 °C (All lines have received B-spline curve processing)

Due to the similarity of the three tested fluids, the above typical results can be obtained in both R134a and R1234ze(E). However, in identical operating conditions, R1234yf, R134a and R1234ze(E) still have different specific flow behaviours. As shown in Fig. 13a, at the condition of $t_g$ = 86 °C, $t_c$ = 40 °C and $t_e$ = 5 °C, the inlet and outlet pressures of these saturated refrigerants are different. At any point along the axis of the ejector, the static pressure of R1234ze(E) is always the minimum, while R134a and R1234yf are approximated.

From Fig. 13b, mass of the three working fluids are almost identical before the primary flow and secondary flow start mixing. Combined with Fig. 12a, therefore, different operating conditions and refrigerants do not change the velocity of the primary fluid at the suction nozzle exit. In addition, as discussed in previous section, $\dot{m}_{pri}$ of R1234yf is close to that of R134a but higher than that of R1234ze(E) at the same

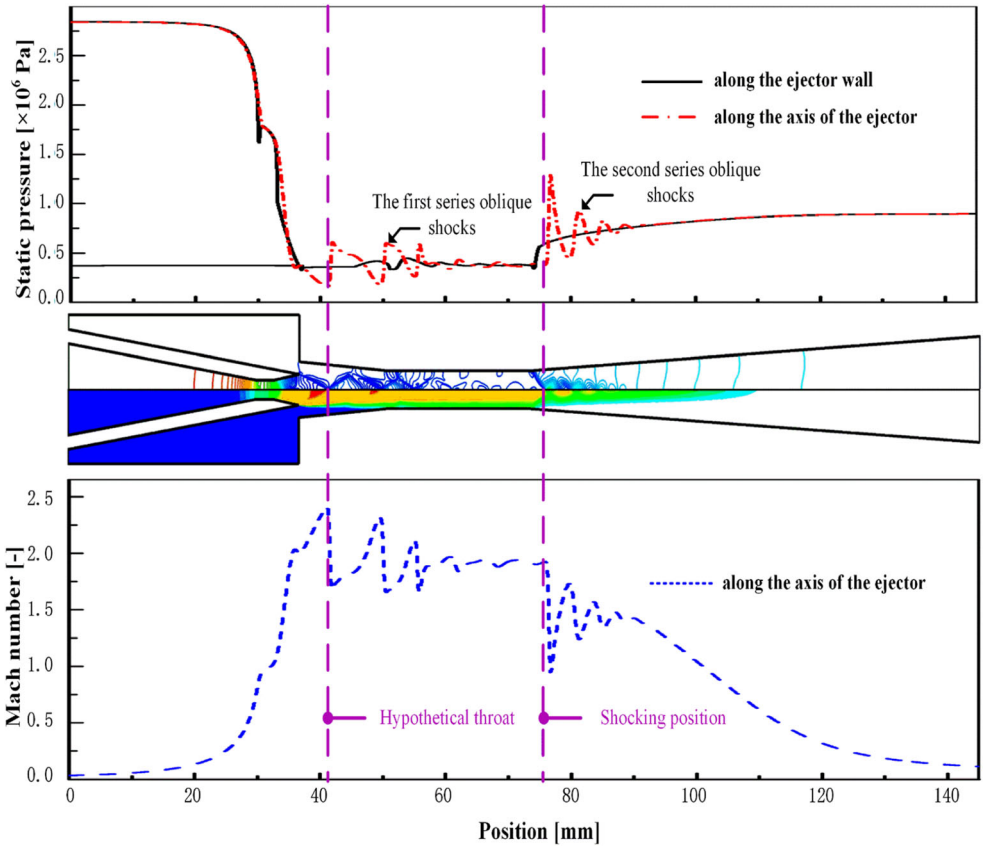


**Fig. 10** Static pressure and Mach number distributions of the ejector

temperature condition. There is a similar trend with $\dot{m}_{pri}$ for the momentum of the primary-fluid jet.

Figure 13c shows the hypothetical throats of R134a and R1234ze(E) appear at almost the same position, but that of R1234yf appears earlier. Therefore, R1234yf has larger expansion angle and effective area than R1234ze(E). In addition, at the downstream of the constant-area section, the shocking position of R1234yf appears earlier than that of R134a or R1234ze(E). Due to this difference, R1234yf always enters the subcritical mode firstly when the operating conditions change. This result indirectly explains the conclusion in previous sections that R1234yf has a smaller critical condenser temperature and operation range of $t_g$ than R134a and R1234ze(E).

In conclusion, there is a typical law for each refrigerant operating at the critical mode. Increasing $t_g$ can make the shocking position and hypothetical throat move downstream. A higher $t_e$ causes the shocking position to move downstream, but the hypothetical throat moves upstream. An increase in $t_c$ makes the shocking position move upstream with an unchanged hypothetical throat position. However, differences remain among the three refrigerants at the same temperature condition, mainly due to different boundary pressures, physical properties, and coupling relationships among these variables.

## Heat transfer of the ejector

Unlike the compressor that consumes external energy in the compressor refrigeration system, pressure increase in the secondary fluid is achieved by the energy transfer of the primary fluid. Ejection efficiency ($\eta$) is introduced to characterize the energy conversion in the ejector. It is defined as the ratio of the effective energy obtained by the secondary fluid and that consumed by the primary fluid per unit time. The effective work of the secondary fluid is the energy that increases the absolute static pressure of the secondary fluid from $P_{sec}$ to $P_{out}$, namely

$$E_2 = q_{sec}\left[\left(P_{out} + \frac{1}{2}\rho_{sec}u_{out}^2\right) - \left(P_{sec} + \frac{1}{2}\rho_{sec}u_{sec}^2\right)\right] \quad (9)$$

where $P_{sec}$ is the inlet pressure of the secondary fluid. $P_{out}$ is the outlet pressure of the mixed fluid. $u_{sec}$ is the inlet viscosity of the secondary fluid. $u_{out}$ is the outlet velocity of the mixed fluid. $\frac{1}{2}\rho_{sec}u_{out}^2 - \frac{1}{2}\rho_{sec}u_{sec}^2$ is the momentum increment of the secondary fluid, which is often not available because of its small value. The effective energy obtained by the secondary fluid is abbreviated as

$$E_2 = q_{sec}(P_{out} - P_{sec}) \quad (10)$$

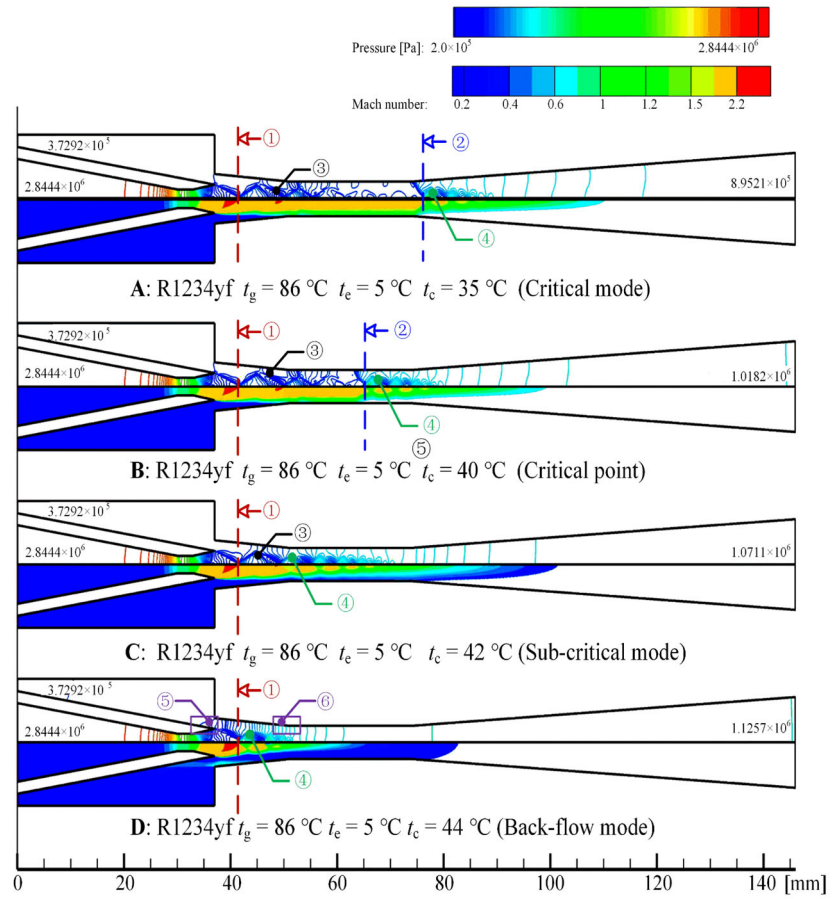


**Fig. 11** The **(a)** Mach number and pressure contours of the ejectors under three working modes (① Hypothetical throat, ② Shocking position, ③ The first series oblique shocks, ④ The second series oblique shocks, ⑤ The reversed flow: Example 1, ⑥ The reversed flow: Example 2) and **(b)** two examples about the reversed flow when the ejector is operating in the back-flow mode

The energy consumed by the primary fluid from the hypothetical throat to the outlet is

$$E_1 = q_{\text{pri}}\left[\left(P_{\text{con}} + \frac{1}{2}\rho_{\text{pri}}u_{\text{exit}}^2\right) - \left(P_{\text{out}} + \frac{1}{2}\rho_{\text{pri}}u_{\text{out}}^2\right)\right] \quad (11)$$

where $P_{\text{con}}$ is the pressure of the primary fluid at the entrance of constant-area, which is equal to the hypothetical throat pressure under constant pressure mixing. $u_{\text{exit}}$ is the velocity of the primary fluid at the nozzle exit. Compared to $u_{\text{exit}}^2$, $u_{\text{out}}^2$ is small enough to be ignored. The energy consumed by the primary fluid is written as

$$E_1 = q_{\text{pri}}\left[\frac{1}{2}\rho_{\text{pri}}u_{\text{exit}}^2 - (P_{\text{out}} - P_{\text{con}})\right] \quad (12)$$

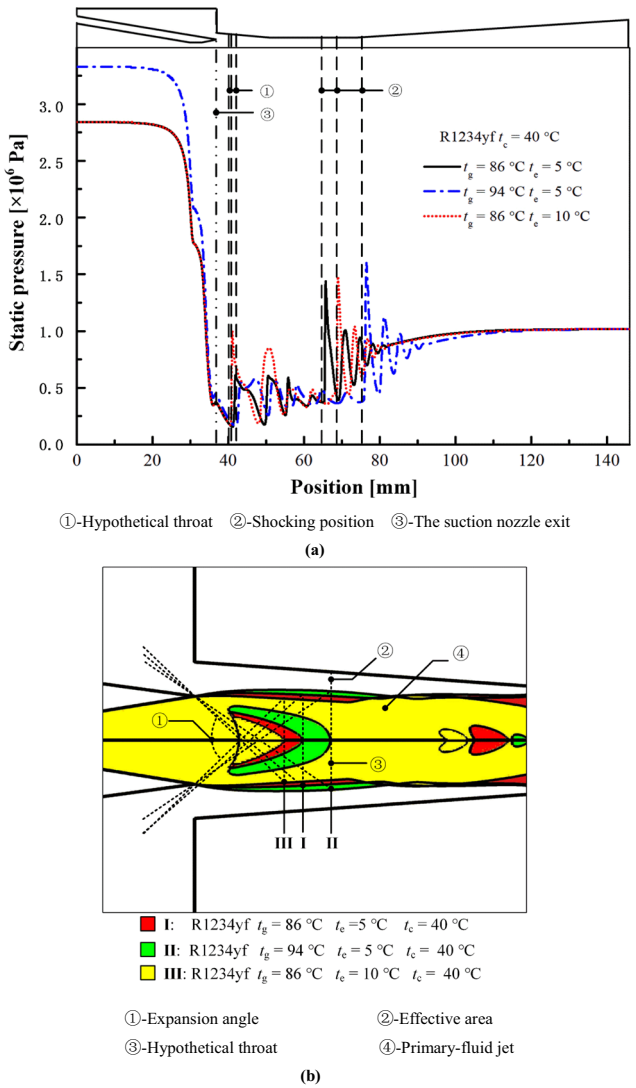


**Fig. 12** The **(a)** static pressure distributions along the axis of the ejectors (① Hypothetical throat, ② Shocking position, ③ The suction nozzle exit) and **(b)** comparisons of the expansion angle of the ejectors operating in three conditions (① Expansion angle, ② Effective area, ③ Hypothetical throat, ④ Primary-fluid jet)

Then, the ejector efficiency (Liu 1980) is marked as

$$\eta = \frac{E_2}{E_1} = \frac{q_{\text{sec}}(P_{\text{out}} - P_{\text{sec}})}{q_{\text{pri}}\left[\frac{1}{2}\rho_{\text{pri}}u_{\text{exit}}^2 - (P_{\text{out}} - P_{\text{con}})\right]} \times 100\% \quad (13)$$

As displayed in Table 7, R1234yf still has an obvious advantage in terms of ejection efficiency under the given operating condition ($t_g$ = 86 °C, $t_c$ = 35 °C and $t_e$ = 5 °C).

It should be noted that there is temperature fluctuation near the surface of an ejector when the high-temperature primary fluid entrains the low-temperature secondary fluid. In the study of Kim and Jeong (2012), the existence of a temperature gradient could cause thermal stress on the ejector surface. When the range of thermal stress is

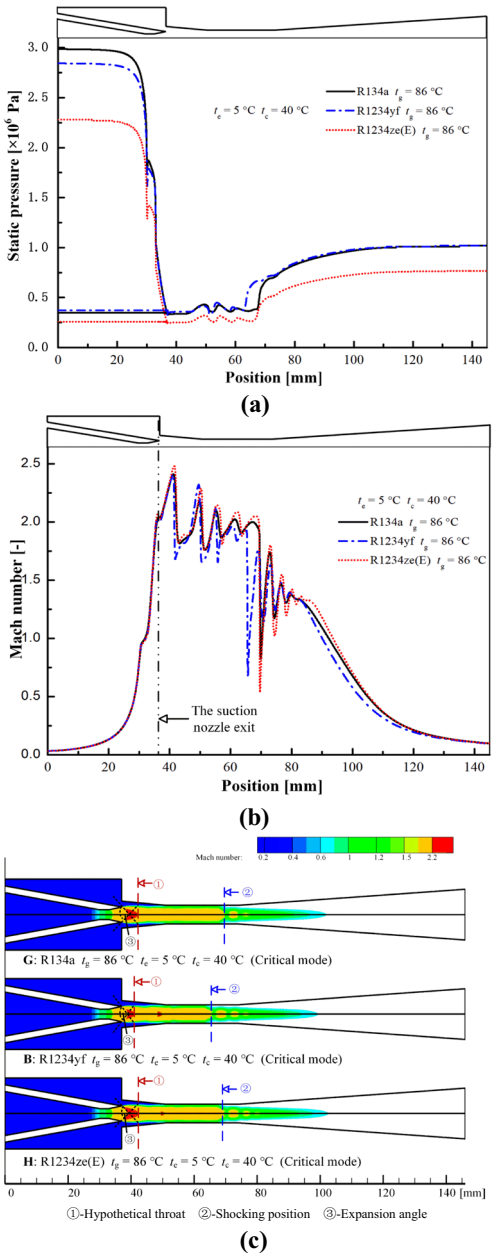


**Fig. 13** Comparisons of flow behaviour that includes the **(a)** static pressure distributions, **(b)** Mach number distributions and **(c)** Mach number contours of the ejectors utilizing three refrigerants (① Hypothetical throat, ② Shocking position, ③ Expansion angle)

sufficiently large, thermal fatigue (thermal striping) that could shorten the life of the ejector and reduce the ejection efficiency will occur. In order to analyse the wall flow and heat transfer of the component, the ejector using R1234yf under the condition of $t_g$ = 86 °C, $t_e$ = 5 °C are performed. As depicted in Fig. 14a, there are swirls appearing in the mixing section and constant-area section of the ejector. A swirl in the mixing section can disturb the laminar flow of primary fluid and secondary fluid, which causes the two fluids to start mixing. A swirl in

**Table 7** Operating parameters and performance indicators for the three refrigerants

| Refrigerant | $q_{pri}$ [$\times 10^{-4}$ $m^3$/s] | $q_{sec}$ [$\times 10^{-4}$ $m^3$/s] | $P_{out}$ [$\times 10^5$ Pa] | $P_{sec}$ [$\times 10^5$ Pa] | $P_{con}$ [$\times 10^5$ Pa] | $\rho$ [kg/$m^3$] | $u_{exit}$ [m/s] | $\eta$ [%] |
|---|---|---|---|---|---|---|---|---|
| R134a | 6.87 | 9.81 | 8.75 | 3.45 | 4.97 | 102 | 343.31 | 13.63 |
| R1234yf | 6.45 | 9.84 | 8.84 | 3.68 | 5.78 | 109 | 321.24 | 15.01 |
| R1234ze(E) | 6.89 | 9.63 | 6.59 | 2.56 | 3.63 | 77.9 | 339.08 | 13.66 |

the constant-area section is caused by the sudden increase of cross-section, which is conducive to the full mixing. The existence of swirls proves the presence of shock waves that cause the fluctuation of the static pressure and Mach number. Besides, swirls can also affect the temperature distribution along the ejector wall. As shown in Fig. 14b, the temperature along the ejector wall does not change before the two fluids are mixed, and it slowly increases after fully mixing. The colours of the two sections are almost unchanged, as shown in Fig. 14c. However, from the hypothetical throat to the shocking position, the temperature along the ejector wall increases rapidly or fluctuates irregularly, and there is colour gradient explaining energy transfer. It can be seen from Fig. 14c that this area is band-shaped and tends to be smaller with the fluid moving downstream. In addition, the hypothetical throat is the position where the temperature fluctuates most, and where thermal fatigue occurs easily.

In Fig. 15, the wall temperature distributions of the three working fluids under a given working condition are compared. For R134a, R1234yf and R1234ze(E), the wall temperature sharply turns and the temperature fluctuates at basically the same location. Although the average temperatures at the surface of the mixing section are different, the temperature fluctuations have a similar trend. Thus, the selection of the working fluid among the three refrigerants hardly affects the life of the ejector.

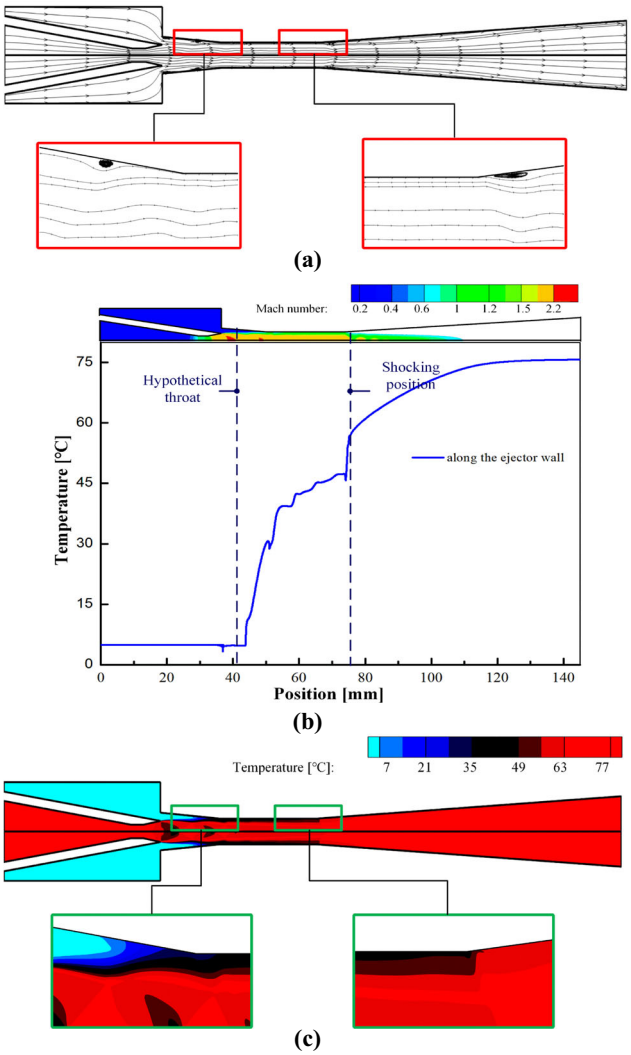


**Fig. 14** The display of inner flow behaviour that includes **(a)** the streamline, **(b)** the temperature distribution along the ejector wall and **(c)** the filled contour of temperature of the ejector

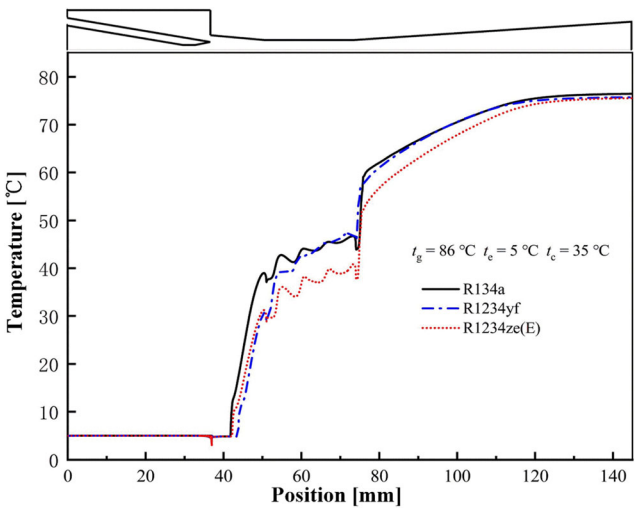


**Fig. 15** Comparisons of temperature distributions along the ejectors wall utilizing three refrigerants

## Conclusions

In this paper, the effects of the condenser temperature, generator temperature and evaporator temperature on the ejector performance are investigated. R1234yf and R1234ze(E) are employed as direct substitutes for R134a to obtain their similarities and differences. The primary conclusions are summarized as follows.

(1) The ejector performance is sensitive to the working temperatures, and this effect is independent of refrigerants. $T_c$ mainly affects the position of the shocking position, which makes $\omega$ maintain the maximum value until $T_c$ increases to the critical value. Increasing $T_g$ under critical mode can lead to a sufficiently expanding primary fluid entraining less secondary fluid, which makes $\omega$ decrease. The increasing $T_e$ can increase $\omega$ by influencing $\dot{m}_{sec}$ without any change in the suction nozzle.
(2) R1234yf always has a greater $\omega$ than R134a and R1234ze(E), which is mainly due to the different saturated pressures of the three working fluids at the same temperature. However, the earlier shocking position makes R1234yf has a smaller critical mode region. Despite this, R1234yf exhibits better ejector performance due to the difference of no more than 3 °C.
(3) Mixing primary and secondary fluids at different temperatures can bring the temperature fluctuation appearing on the surface of an ejector. The wall temperature most drastically changes near the location of the hypothetical throat and shocking position, in which the two fluids start mixing or well-mixed. The existence of temperature fluctuations proves the presence of shock waves that cause the fluctuation of the static pressure and Mach number.

In the present work, only the internal flow behaviours of different working fluids under identical temperature conditions are compared. Further research is required on the effects of specific physical properties on the ejector performance. For example, the thermal conductivity, specific heat capacity and viscosity of the fluid can affect its thermal diffusivity. It is necessary to analyse the relationship between these physical properties and the entrainment ratio, expansion angle, shock waves and other flow behaviours in the ejector. Thence, a new type of working fluid, with better physical properties for better ejector performance, can be prepared by using the existing refrigerants.

**Nomenclature** $E$, Total energy, [J]; $e$, Difference of the mass flow rate between two grides, [kg/s]; $F$, Safety factor, [-]; $GCI$, Grid convergence index, [-]; $\dot{m}$, Mass flow rate, [kg/s]; $P$, Pressure, [Pa]; $p$, Order of the convergence, [-]; $q$, Volume flow, [m3/s]; $r$, Refinement ratio, [-]; $t$, Temperature, [°C]; $T$, Static temperature, [K]; $u$, Velocity vector, [m/s]; $x$, Cartesian coordinates, [-]

**Greek symbols** $\omega$, Entrainment ratio, [-]; $\eta$, Ejection efficiency, [-]; $\rho$, Density, [kg/m3]; $\delta ij$, Kronecker delta, [-]; $\kappa eff$, Thermal conductivity, [W/(m·K)]; $\mu eff$, Dynamic viscosity, [(N·s)/m2]; $\omega$, Entrainment ratio, [-]; $\eta$, Ejection efficiency, [-]; $\rho$, Density, [kg/m3]; $\delta ij$, Kronecker delta, [-]; $\kappa eff$, Thermal conductivity, [W/(m·K)]; $\mu eff$, Dynamic viscosity, [(N·s)/m2]

**Subscripts** c, Condenser; CFD, CFD model; con, The entrance of the constant-area; e, Evaporator; exit, The Nozzle exit; exp, Experiment; g, Generator; out, Outlet; pri, The primary fluid; sec, The secondary fluid

**Author contribution** All authors contributed to the study conception and design. Material preparation, data collection and analysis were performed by [Shizhen Li], [Jingzhi Zhang], [Yingxin Liu] and [Yanjun Liu]. The first draft of the manuscript was written by [Yingxin Liu] and all authors commented on previous versions of the manuscript. All authors read and approved the final manuscript.

**Funding** This work is supported by the [National Natural Science Foundation of China] under Grant [51705288], [Shandong Provincial Natural Science Foundation] under Grant [ZR2017QEE001, ZR2018BEE026]; [Shandong Provincial Key R&D Program Foundation] under Grant [2018GHY115006, 2019GSF109051]; and [National Key R&D Program of China] under Grant [2016YFE0205700].

**Data availability** Not applicable.

## Declarations

**Ethics approval and consent to participate** Not applicable.

**Consent for publication** Not applicable.

**Competing interests** The authors declare no competing interests.

## References

Atmaca AU, Erek A, Ekren OJEP (2017) Investigation of new generation refrigerants under two different ejector mixing theories. Energy Procedia. 136:394–401. https://doi.org/10.1016/j.egypro.2017.10.271

Bartosiewicz Y, Aidoun Z, Desevaux P, Mercadie Y (2005) Numerical and experimental investigations on supersonic ejectors. Int J Heat Fluid Fl 26(1):56–70. https://doi.org/10.1016/j.ijheatfluidflow.2004.07.003

Besagni G, Cristiani N, Croci L, Guédon GR, Inzoli F (2020a) Computational fluid-dynamics modelling of supersonic ejectors: screening of modelling approaches, comprehensive validation and assessment of ejector component efficiencies. Appl Therm Eng 186:116431. https://doi.org/10.1016/j.applthermaleng.2020.116431

Besagni G, Cristiani N, Croci L, Guédon GR, Inzolia F (2020b) Multi-scale evaluation of ejector performances: the influence of refrigerants and ejector design. Appl Therm Eng 186:116502. https://doi.org/10.1016/j.applthermaleng.2020.116502

Biferi G, Giacomelli F, Mazzelli F, MilazzoA (2016) CFD modelling of the condensation inside a supersonic ejector working with R134a. Energy Procedia 101:1232–1239. https://doi.org/10.1016/j.egypro.2016.11.138

Cheng Y, Wang M, Yu JL (2021) Thermodynamic analysis of a novel solar-driven booster-assisted ejector refrigeration cycle. Sol Energy 218(17):85–94. https://doi.org/10.1016/j.solener.2021.02.031

Chunnanond K, Aphornratana S (2004) An experimental investigation of a steam ejector refrigerator: the analysis of the pressure profile along the ejector. Appl Therm Eng 24(2-3):311–322. https://doi.org/10.1016/j.applthermaleng.2003.07.003

Croquer S, Poncet S, Aidoun Z (2016) Turbulence modelling of a single-phase R134a supersonic ejector. Part 1: Numerical benchmark. Int J Refrig 61:140–152. https://doi.org/10.1016/j.ijrefrig.2015.07.030

Elakhdar M, Tashtoush BM, Nehdi E, Kairouani L (2018) Thermodynamic analysis of a novel ejector enhanced vapor compression refrigeration (EEVCR) cycle. Energy 163:1217–1230. https://doi.org/10.1016/j.energy.2018.09.050

Expósito Carrillo JA, Sánchez de La Flor FJ, Salmerón Lissén JM (2017) Thermodynamic comparison of ejector cooling cycles. ejector characterisation by means of entrainment ratio and compression efficiency. Int J Refrig 74:371–384. https://doi.org/10.1016/j.ijrefrig.2016.11.006

Fang Y, Croquer S, Poncet S, Aidoun Z, Bartosiewicz Y (2017) Drop-in replacement in a R134 ejector refrigeration cycle by HFO refrigerants. Int J Refrig 77:87–98. https://doi.org/10.1016/j.ijrefrig.2017.02.028

Galindo J, Dolz V, García-Cuevas LM, Ponce-Mora A (2020) Numerical evaluation of a solar-assisted jet-ejector refrigeration system: screening of environmentally friendly refrigerants. Energ Convers Manage 210:112681. https://doi.org/10.1016/j.enconman.2020.112681

García del Valle J, Saíz Jabardo JM, Castro Ruiz F, San José Alonso JF (2014) An experimental investigation of a R-134a ejector refrigeration system. Int J Refrig 46:105–113. https://doi.org/10.1016/j.ijrefrig.2014.05.028

Gu WD, Wang L, Wang XL (2017) Area ratio optimization of an ejector refrigeration system with water-cooled condenser. 2017 Chinese Automation Congress (CAC)

Han Y, Wang X, Sun H, Zhang G, Guo L, Tu J (2019) CFD simulation on the boundary layer separation in the steam ejector and its influence on the pumping performance. Energy 167:469–483. https://doi.org/10.1016/j.energy.2018.10.195

He S, Li Y, Wang RZ (2009) Progress of mathematical modelling on ejectors. Renew Sust Energ Rev 13(8):1760–1780. https://doi.org/10.1016/j.rser.2008.09.032

Huang BJ, Chang JM, Wang CP, Petrenko VA et al (1999) A 1-D analysis of ejector performance. Int J Refrig 22(5):354–364. https://doi.org/10.1016/S0140-7007(99)00004-3

John WS (2021) Examining Spatial (Grid) Convergence. IOP Publishing Physics Web. https://www.grc.nasa.gov/WWW/wind/valid/tutorial/spatconv.html. Accessed 1 May 2021

Keenan J Neumann E (1950) An investigation of ejector design by analysis and experiment.

Kim JK, Jeong JJ (2012) Large eddy simulation of turbulent flow in a T-junction. Numer Heat Tr A-Appl 61(3):180–200. https://doi.org/10.1080/10407782.2012.644167

Kumar K, Gupta HK, Kumar P (2020) Analysis of a hybrid transcritical $CO_2$ vapor compression and vapor ejector refrigeration system. Appl Therm Eng 181:115945. https://doi.org/10.1016/j.applthermaleng.2020.115945

Lemmon EW, Huber ML, McLinden MO (2013) NIST standard reference database 23: reference fluid thermodynamic and transport properties-REFPROP, version 9.1. NIST NSRDS

Liu RD (1980) Metallurgy furnace thermal engineering basis. Metallurgical Industry Press, Beijing, p 107

Mahmoudian J, Mazzelli F, Rocchetti A, Milazzo A (2020) A heat-powered ejector chiller working with low-gwp fluid R1233zd(E) (part2: numerical analysis). Int J Refrig. 121:216–227. https://doi.org/10.1016/j.ijrefrig.2020.10.016

Mazzelli F, Little AB, Garimella S, Bartosiewicz Y (2015) Computational and experimental analysis of supersonic air ejector: Turbulence modelling and assessment of 3D effects. Int J Heat Fluid Fl 56:305–316. https://doi.org/10.1016/j.ijheatfluidflow.2015.08.003

Mazzelli F, Giacomelli F, Milazzo A (2018) CFD modeling of condensing steam ejectors: comparison with an experimental test-case. Int J Therm Sci 127:7–18. https://doi.org/10.1016/j.ijthermalsci.2018.01.012

Megdouli K, Tashtoush BM, Nahdi E, Elakhdar M, Kairouani L (2017) Performance analysis of a combined vapor compression cycle and ejector cycle for refrigeration cogeneration. Int J Refrig 74:515–525. https://doi.org/10.1016/j.ijrefrig.2016.12.003

Metin C, Gok O, Atmaca AU, Erek A (2019) Numerical investigation of the flow structures inside mixing section of the ejector. Energy 166:1216–1228. https://doi.org/10.1016/j.energy.2018.10.095

Mondal S, De S (2020) Performance assessment of a low-grade heat driven dual ejector vapour compression refrigeration cycle. Appl Therm Eng 179:115782. https://doi.org/10.1016/j.applthermaleng.2020.115782

Munday JT, Bagster DF (1977) A new ejector theory applied to steam jet refrigeration. Ind Eng Chem Res 16(4):442–449. https://doi.org/10.1021/i260064a003

Mwesigye A, Dworkin SB (2018) Performance analysis and optimization of an ejector refrigeration system using alternative working fluids under critical and subcritical operation modes. Energ Convers Manage 176:209–226. https://doi.org/10.1016/j.enconman.2018.09.021

Oliveira Marum VJD, Reis LB, Maffei FS, Ranjbarzadeh S, Korkischko I, Santos Gioria RD, Meneghini JR (2021) Performance analysis of a water ejector using computational fluid dynamics (CFD) simulations and mathematical modeling. Energy. 220:119779. https://doi.org/10.1016/j.energy.2021.119779

Pabon JJG, Khosravi A, Belman-Flores JM, Machado L, Revellin R (2020) Applications of refrigerant R1234yf in heating, air conditioning and refrigeration systems: a decade of researches. Int J Refrig 118:104–113. https://doi.org/10.1016/j.ijrefrig.2020.06.014

Pérez BP, Expósito Carrillo JA, Sánchez de La Flor FJ et al (2021) Thermoeconomic analysis of $CO_2$ ejector-expansion refrigeration cycle (EERC) for low-temperature refrigeration in warm climates. Appl Therm Eng 188(6):116613. https://doi.org/10.1016/j.applthermaleng.2021.116613

Petrovic A, Jovanovic MZ, Genic S, Bugaric U, Delibasic B (2018) Evaluating performances of 1-D models to predict variable area supersonic gas ejector performances. Energy 163(15):270–289. https://doi.org/10.1016/j.energy.2018.08.115

Rogdakis ED, Alexis GK (2000) Design and parametric investigation of an ejector in an air-conditioning system. Appl Therm Eng 20(2):213–226. https://doi.org/10.1016/S1359-4311(99)00013-7

Sanaye S, Emadi M, Refahi A (2019) Thermal and economic modeling and optimization of a novel combined ejector refrigeration cycle. Int J Refrig 98:480–493. https://doi.org/10.1016/j.ijrefrig.2018.11.007

Sieres J, Santos JM (2018) Experimental analysis of R1234yf as a drop-in replacement for R134a in a small power refrigerating system. Int J Refrig 91:230–238. https://doi.org/10.1016/j.ijrefrig.2018.05.019

Sokolov M, Hershgal D (1991) Enhanced ejector refrigeration cycles powered by low grade heat. part 3. experimental results. Int J Refrig 14(1):24–31. https://doi.org/10.1016/0140-7007(91)90018-C

Sriveerakul T, Aphornratana S, Chunnanond K (2007) Performance prediction of steam ejector using computational fluid dynamics: part 2. flow structure of a steam ejector influenced by operating pressures

and geometries. Int J Therm Sci 46(8):823–833. https://doi.org/10.1016/j.ijthermalsci.2006.10.012

Tang YZ, Liu ZL, Li YX, Huang ZF, Chua KJ (2020) Study on fundamental link between mixing efficiency and entrainment performance of a steam ejector. Energy 20201(215):119128. https://doi.org/10.1016/j.energy.2020.119128

Union P, Parliament TE Euro TCOT (2006) directive 2006/38/ec of the european parliament and of the council of 17 May 2006. https://eur-lex.europa.eu/LexUriServ

Varga S, Lebre PMS, Oliveira AC (2013) CFD study of a variable area ratio ejector using R600a and R152a refrigerants. Int J Refrig 36(1):157–165. https://doi.org/10.1016/j.ijrefrig.2012.10.016

Wang L, Liu JP, Zou T, Du JW, Jia FZ (2018) Auto-tuning ejector for refrigeration system. Energy. 161:536–543. https://doi.org/10.1016/j.energy.2018.07.110

Yan J, Cai W, Li Y (2012) Geometry parameters effect for air-cooled ejector cooling systems with R134a refrigerant. Renew Energ 46:155–163. https://doi.org/10.1016/j.renene.2012.03.031

Yilmaz T, Erdinç MT (2019) Energetic and exergetic investigation of a novel refrigeration system utilizing ejector integrated subcooling using different refrigerants. Energy 168:712–727. https://doi.org/10.1016/j.energy.2018.11.081